Flinders
UNIVERSITY

The following article appeared as:

Gascooke, J.R., Alexander, U.N. and Lawrance, W.D., 2011. Two dimensional laser induced fluorescence spectroscopy: a powerful technique for elucidating rovibronic structure in electronic transitions of polyatomic molecules. Journal of Chemical Physics, 134, 184301.

and may be found at:
http://jcp.aip.org/resource/1/jcpsa6/v134/i18/p184301_s1

DOI: http://dx.doi.org/10.1063/1.3578174

Two dimensional laser induced fluorescence spectroscopy: A powerful technique for elucidating rovibronic structure in electronic transitions of polyatomic molecules

Jason R. Gascooke, Ula N. Alexander, and Warren D. Lawrance

Citation: J. Chem. Phys. **134**, 184301 (2011); doi: 10.1063/1.3578174
View online: http://dx.doi.org/10.1063/1.3578174
View Table of Contents: http://jcp.aip.org/resource/1/JCPSA6/v134/i18
Published by the American Institute of Physics.

Two dimensional laser induced fluorescence spectroscopy: A powerful technique for elucidating rovibronic structure in electronic transitions of polyatomic molecules

Jason R. Gascooke, Ula N. Alexander, and Warren D. Lawrance[a)]
School of Chemical and Physical Sciences, Flinders University, GPO Box 2100, Adelaide, South Australia 5001, Australia

(Received 20 December 2010; accepted 9 March 2011; published online 9 May 2011)

We demonstrate the power of high resolution, two dimensional laser induced fluorescence (2D-LIF) spectroscopy for observing rovibronic transitions of polyatomic molecules. The technique involves scanning a tunable laser over absorption features in the electronic spectrum while monitoring a segment, in our case 100 cm^{-1} wide, of the dispersed fluorescence spectrum. 2D-LIF images separate features that overlap in the usual laser induced fluorescence spectrum. The technique is illustrated by application to the S_1–S_0 transition in fluorobenzene. Images of room temperature samples show that overlap of rotational contours by sequence band structure is minimized with 2D-LIF allowing a much larger range of rotational transitions to be observed and high precision rotational constants to be extracted. A significant advantage of 2D-LIF imaging is that the rotational contours separate into their constituent branches and these can be targeted to determine the three rotational constants individually. The rotational constants determined are an order of magnitude more precise than those extracted from the analysis of the rotational contour and we find the previously determined values to be in error by as much as 5% [G. H. Kirby, Mol. Phys. **19**, 289 (1970)]. Comparison with earlier *ab initio* calculations of the S_0 and S_1 geometries [I. Pugliesi, N. M. Tonge, and M. C. R. Cockett, J. Chem. Phys. **129**, 104303 (2008)] reveals that the CCSD/6–311G** and RI-CC2/def2-TZVPP levels of theory predict the rotational constants, and hence geometries, with comparable accuracy. Two ground state Fermi resonances were identified by the distinctive patterns that such resonances produce in the images. 2D-LIF imaging is demonstrated to be a sensitive method capable of detecting weak spectral features, particularly those that are otherwise hidden beneath stronger bands. The sensitivity is demonstrated by observation of the three isotopomers of fluorobenzene-d_1 in natural abundance in an image taken for a supersonically cooled sample. The ability to separate some of the ^{13}C isotopomers in natural abundance is also demonstrated. The equipment required to perform 2D-LIF imaging with sufficient resolution to resolve the rotational features of large polyatomics is available from commercial suppliers. © *2011 American Institute of Physics*. [doi:10.1063/1.3578174]

I. INTRODUCTION

Gas phase electronic spectra of polyatomics often combine a richness of features with a structure that is complicated in its interpretation by effects including vibronic coupling and anharmonic and Coriolis interactions. Consequently, there is increasing interest in developing new, multidimensional spectroscopic techniques to provide deeper insights when interrogating and assigning molecular electronic spectra. The development of multidimensional techniques is a natural consequence of advances in detection methodologies and is an area emerging more widely for spectroscopic and molecular dynamics measurements, including the time domain.[1–4]

Chen has recently summarized advances in high resolution coherent two dimensional (2D) approaches for interrogating complex rovibronic spectra in the UV/visible region for gas phase samples.[3] In contrast to the multiple laser approach, Reilly, Schmidt, and Kable demonstrated that combining dispersed fluorescence and laser induced fluorescence (LIF) scanning into a single 2D spectral measurement provides a powerful method for identifying fluorescing species in complex chemical environments.[5] Their single laser technique involves measuring the dispersed fluorescence spectrum at each laser wavelength in an LIF scan. The LIF was collected and dispersed using a spectrometer with a charge couple device (CCD) array detector allowing a large region of the fluorescence spectrum to be captured at each laser position, albeit at limited resolution. By plotting the fluorescence intensity as a function of the excitation and emission wavelengths (hence 2D fluorescence), they were able to readily identify the emitting species where the spectrum was known.

While Reilly, Schmidt, and Kable used the 2D approach to identify molecular species from their known spectra, this 2D fluorescence approach has obvious and straightforward application to vibronic spectral assignment for electronic transitions in polyatomics. Observation of the dispersed fluorescence spectrum at each laser position means that it is measured for each LIF spectral feature, providing a means to assign the feature based on known ground state vibrational

a)Author to whom correspondence should be addressed: Electronic mail: warren.lawrance@flinders.edu.au.

frequencies. This is essentially a straightforward extension of the more usual approach of measuring an LIF spectrum and separately measuring dispersed fluorescence spectra from selected features. A less obvious application of the technique is the measurement of rotational "contours" in two dimensions as an extension of the usual band contour analysis for extracting rotational constants. Expanding on the work by Reilly, Schmidt, and Kable we have developed the 2D fluorescence probe for higher resolution interrogation of molecular spectra, particularly for application to "large" polyatomic molecules. We illustrate the technique by application to the S_1–S_0 transition in fluorobenzene. In this context the complex spectroscopy of a polyatomic molecule mimics the complex chemical environment probed by Reilly, Schmidt, and Kable. We show that 2D imaging is a sensitive method capable of detecting weak spectral features, including those that are otherwise hidden beneath stronger bands. We have found that a particular advantage of 2D imaging is that it separates the rotational contours into constituent branches that can be targeted to determine the three rotational constants without the need for approximations such as that of planarity. Moreover, in 2D features that overlap in the usual LIF spectrum can be separated with, for example, sequence bands no longer interfering with the rotational structure of the cold bands. Because position sensitive photon detectors such as image intensifiers can be as sensitive as photomultipliers, effectively working at the single photon detection limit, the 2D imaging technique can remain a sensitive technique.

In order to differentiate the 2D imaging technique from the familiar LIF (where typically the total fluorescence is detected as a function of laser wavelength) and dispersed fluorescence (where the fluorescence spectrum is collected at a single laser wavelength), we introduce the term "2D laser induced fluorescence" (2D-LIF) to describe the two dimensional images arising from collecting dispersed fluorescence while scanning the laser wavelength.

Although the spectroscopy of benzene and its derivatives has been studied extensively, there have been surprisingly few studies of the S_1–S_0 transition of fluorobenzene using modern techniques, especially given its focus in studies of van der Waals complexes.[6–8] Lipp and Seliskar undertook an extensive study of the S_1–S_0 absorption spectrum, including deuterated species, using conventional absorption with room temperature samples.[9,10] Gonohe *et al.* reported the first LIF spectrum and selected dispersed fluorescence spectra of a jet cooled sample.[11] However, it was not until 2007 that Butler *et al.* published an extensive investigation of jet-cooled fluorobenzene using a combination of LIF and dispersed fluorescence to identify and assign many of the features.[12] They noted that Fermi resonances were extensive throughout the spectrum. Pugliesi *et al.* subsequently examined the S_1 and S_0 vibrations to correlate the normal modes in the two electronic states and to examine the extent to which the Wilson mode numbering and description applies to this simplest of substituted benzenes.[13] These authors published the first resonance enhance multiphoton ionisation (REMPI) spectrum of the S_1–S_0 transition. Recent microwave spectra have produced a very accurate set of constants for the ground state.[14] However, the only rotational analysis of the origin band was reported by Kirby in 1970.[15] It is particularly noteworthy that the S_1 rotational constants have not been re-examined as Kirby noted that two sets of constants could reproduce the segment of the contour that he observed clear from sequence band interference. Given the possibility that the accepted rotational constants, and hence geometry, for S_1 fluorobenzene may be in error, this is a useful system for probing using 2D-LIF.

We have measured the 0_0^0 band region of fluorobenzene at room temperature and cooled to ~7 K in a supersonic free jet expansion. The room temperature study was undertaken with the aim of ascertaining the extent to which the 2D-LIF approach could remove spectral overlap, particularly from sequence bands, and hence reveal the rotational structure at high J, allowing accurate, high precision, rotational constants to be determined. Supersonically cooled spectra do not extend to sufficiently high J to allow highly precise constants to be determined at our laser resolution. The supersonic free jet spectra were measured to illustrate the usefulness of the technique for observing weak features in the fluorobenzene spectrum, particularly the various isotopomers in natural abundance.

II. EXPERIMENTAL DETAILS

The setup for our 2D-LIF experiments is as follows. The frequency doubled output of a Nd:YAG (Continuum Surelite II, 10 Hz repetition rate) was used to pump a dye laser with second harmonic generation (Lambda Physik Scanmate 2E, Coumarin 503 laser dye; 0.3 cm^{-1} doubled linewidth) which, in order to match the geometry of the entrance slit of the spectrometer, passed vertically through a stainless steel chamber containing the source. For the results presented in this work the source was either an effusive expansion of fluorobenzene that was scattered off a stainless steel plate to obtain room temperature spectra or a supersonic free jet expansion of 1% fluorobenzene in argon, sampled at X/D~10, to obtain spectra with vibrational and rotational cooling. At this X/D rotational contour fits indicate a rotational temperature of 7 K. The fluorescence is collected using a lens matched to the f number of a home-built 4.2 m Czerny Turner spectrometer with a 1200 groove/mm grating blazed at 1 μm. In the UV region relevant for the present experiments the spectrometer operates in fourth order with a dispersion of ca. 5 cm^{-1} per mm. The laser wavelength was calibrated using a wavemeter (Bristol Model 821) and scattered laser light was used to calibrate the spectrometer. The dispersed fluorescence is detected with a 25 mm diameter gated image intensifier (Proxitronic BV 2561) with single photon detection sensitivity. Because of a loss of sensitivity at the edges (due to the image intensifier vertical dimension no longer matching the slit height), the effective width of the region viewed is ~100 cm^{-1}. The image intensifier is gated to detect fluorescence in a time window near the laser; the precise timing details depend on the particular experiment being performed and whether or not there is a need to minimize scattered laser light. The image intensifier produces bright spots on a phosphor screen corresponding to the positions where photons strike its front face. The phosphor screen is imaged onto a home-built CCD camera whose output is read each laser shot by a computer. The CCD image is analyzed to identify and record the centre of

each spot observed. This information is used to build up a histogram of events at each camera pixel position. The process continues for a preset number of laser shots while the laser is fixed in wavelength, producing a section of the dispersed fluorescence spectrum at that laser wavelength. The laser then steps to the next wavelength and the process repeats until the laser has scanned the region required. The result is a 3D surface of fluorescence intensity as a function of both the laser and dispersed fluorescence wavelengths. Where long (in time) scans were performed, the 2D-LIF image was recorded multiple times with a low number of laser shots per laser wavelength and the resulting images summed to produce the final image.

The 100 cm^{-1} wide window on the dispersed fluorescence spectrum this setup provides is far narrower than the 6200 cm^{-1} used by Reilly, Schmidt, and Kable[5] and confers the advantage of high resolution. Depending upon the entrance slit width used, the fluorescence resolution can be comparable to that of the laser excitation source.

III. ROOM TEMPERATURE SPECTRA

In this section we present the results of our experiments using a room temperature sample and explore the advantages of high resolution 2D-LIF imaging. We also present the method used to model the image and extract the rotational constants. Throughout this paper we use the Mulliken mode numbering introduced by Butler *et al.* to describe the fluorobenzene vibrational modes.[12] Pugliesi *et al.* have shown that the Wilson mode numbering, which is based on the modes of benzene and used in early fluorobenzene spectroscopy, does not adequately describe all of the normal modes of fluorobenzene.[13]

A. The experimental 2D-LIF image

The 2D-LIF image of the origin region of fluorobenzene at room temperature is shown in Fig. 1. The intensity is displayed using a logarithmic color scale, enabling the majority of features to be clearly observed. Figure 1(b) shows the same image as Fig. 1(a), but with the intensity scale magnified to reveal the weaker features. No image enhancement has been performed. The laser is scanned from 13 cm^{-1} above the fluorobenzene origin band to 81 cm^{-1} below it. The fluorescence is monitored in a 100 cm^{-1} wide window centred at 37 787 cm^{-1} to capture fluorescence transitions in the origin region. At this setting of the spectrometer, the laser wavelength is within the detection window, so the time at which the image intensifier was pulsed on was delayed to exclude scattered laser light.

As this is the first of our 2D-LIF images to be presented, we begin with an explanation of their features. The images are plotted with laser wavenumber along the horizontal axis (termed the excitation axis) and fluorescence wavenumber along the vertical axis (termed the fluorescence axis). By monitoring the origin region in fluorescence, we always observe an emission band at the same wavelength as absorption, and this creates a feature along the line of equal

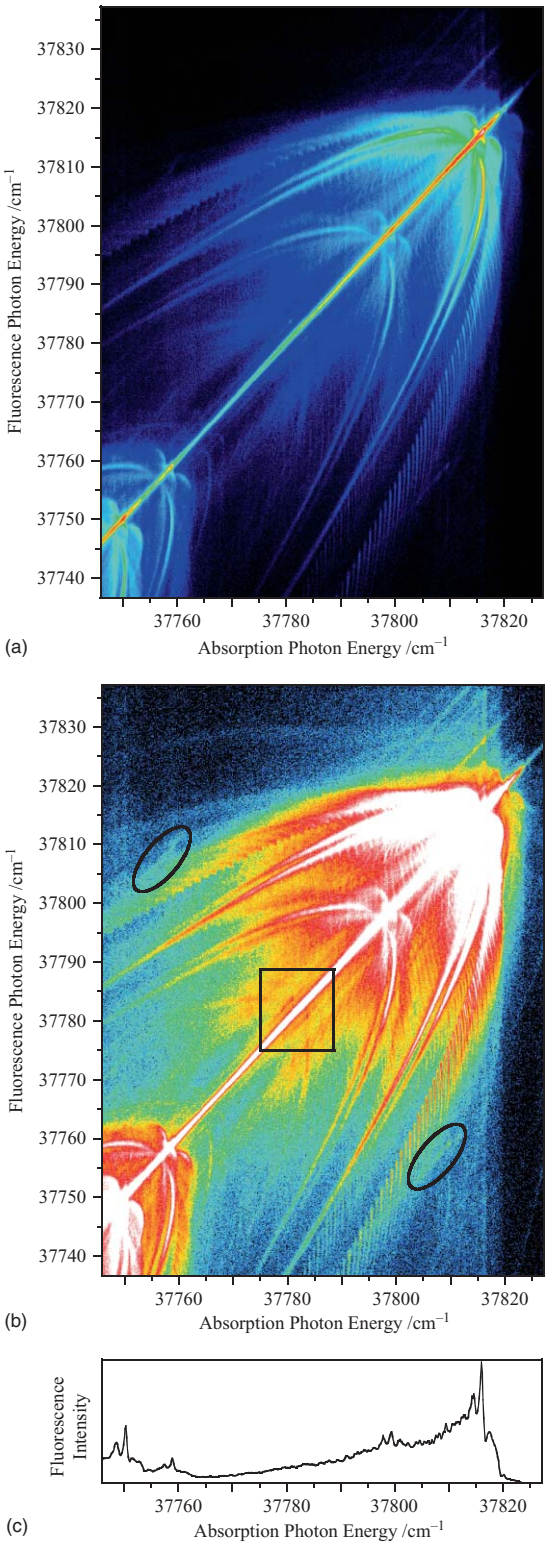

FIG. 1. Two dimensional laser induced fluorescence (2D-LIF) image of a room temperature sample of fluorobenzene. The laser is scanned in the region of the 0_0^0 transition and its sequence structure while the spectrometer is set to detect fluorescence in the same region. The intensity is displayed on a logarithmic scale. (a) and (b) show the same image, but the intensity scale has been magnified in (b) to highlight weaker features. (c) shows the laser induced fluorescence (LIF) spectrum generated by projecting the 2D-LIF image onto the laser (absorption) axis. The ovals marked in image (b) highlight the coupled Fermi resonance features located at (37 809.5, 37 758.9) and (37 758.9, 37 809.5). The rectangular section highlights the observed sequence bands at 37 780.8 cm^{-1} and 37 783.5 cm^{-1}. See Fig. 5 for an enlargement of this region.

absorption/emission wavenumber. We refer to this line as the image diagonal, and it can be clearly seen running from the top right hand corner to the bottom left hand corner in Figs. 1(a) and 1(b). We describe the location of features within an image by their (x, y) coordinates [i.e. (laser wavenumber, fluorescence wavenumber)].

A feature of the 2D-LIF images is the symmetry of the dominant rotational structure about the image diagonal, which is clearly evident in Fig. 1. A point (m, n) in the image corresponding to laser excitation at m cm^{-1} and fluorescence at n cm^{-1} has a corresponding point (n, m) arising from the reverse transition, i.e., laser excitation at n cm^{-1} and fluorescence at m cm^{-1}. This results in reflection symmetry about the image diagonal. The intensities of the two related transitions differ because the initial state is different, resulting in different Boltzmann populations, and the fluorescence intensities will not necessarily be the same (see Sec. III B). Polarization effects may also influence the observed relative intensities of these respective transitions.[16] Examination of Fig. 1 shows that the fluorescence resolution is slightly lower than the excitation resolution and this is seen in features mirrored about the image diagonal being less sharp when their resolution is governed by that of the spectrometer. The symmetry about the image diagonal is also well approximated for detection of other vibronic emission bands where the change in rotational constant generally leads to only a minor perturbation of the contour.

The main feature of the image is the 0_0^0 transition, which has an intense feature at (37 816.0, 37 816.0) and "branches" that sweep back to lower energies on both sides of the image diagonal. These branches are rotational structure that results from the rotational transitions occurring during absorption and fluorescence. Assignments of the more prominent branches are discussed in Sec. III C and the appendix. Shifted along the image diagonal to lower energy are several sequence bands, each displaying the same pattern as 0_0^0. Also contained in the images are several weak 0_0^0-like patterns that are displaced from the image diagonal [see, for example, the features at (37 809.5, 37 758.9) and (37 758.9, 37 809.5) highlighted with an oval in Fig. 1(b)]. These off-diagonal features arise when the vibronic transition in fluorescence differs from the absorption transition. Table I lists the bands observed in the image and their absorption wavenumber (corresponding to the position of maximum intensity for each transition) and assignment. From our fitting of the 0_0^0 transition (see Sec. III C) we determine the peak maximum of 0_0^0 to be blue shifted 2.2 cm^{-1} from the band origin. Lipp and Seliskar,[10] in their fluorobenzene hot band analysis, have published peak positions for observed sequence bands. All features observed in our image are within 0.2 cm^{-1} of the values they reported. Interestingly, we observe two features, with shifts of −32.5 cm^{-1} and −35.2 cm^{-1} from the origin band, not reported by Lipp and Seliskar.[10] Their identities are discussed in Sec. III D. Grating ghosts are seen in the image and appear as a very weak duplication of strong features shifted along the fluorescence axis. They are most readily observed in Fig. 1 to higher fluorescence energy because of reduced overlap with strong features. We have identified the grating ghost shifts using scattered laser light and hence can account for them in assignments.

TABLE I. Assignments of the vibronic features seen in the room temperature 2D-LIF image of fluorobenzene.

Absorption Peak[a]/cm^{-1}	Assignment
37816.0	0_0^0
37809.5 (−6.5)	$11_0^1 20_2^0 \ldots 11_1^1$
37799.3 (−16.7)	30_1^1
37783.5 (−32.5)	$30_2^2 \ldots 10_1^0 30_0^2$
37780.8 (−35.2)	$10_1^0 30_0^2 \ldots 30_2^2$
37758.9 (−57.1)	$11_1^1 \ldots 11_0^1 20_2^0$
37750.2 (−65.8)	20_1^1

[a]Values refer to the peak maximum in the room temperature spectrum. Peak maxima are blue shifted 2.2 cm^{-1} from the band origin. Values in parentheses indicate the shift from the origin transition.

The data in Figs. 1(a) and 1(b) are easily transformed into the more familiar LIF spectrum by projecting the image onto the absorption axis, and this is shown in Fig. 1(c). The features of the 0_0^0 transition in this LIF spectrum match those presented by Kirby in his room temperature absorption study.[15] Comparing Figs. 1(a) and 1(c), it is evident that the 2D-LIF image has some clear advantages over the 1D-LIF spectrum. An issue with room temperature spectra of large polyatomics is the presence of sequence bands that overlap cold bands, complicating assignments and obscuring features, as can be seen in Fig. 1(c). The 2D-LIF technique separates these contributions. Rotational branches associated with the 0_0^0 band appear in a different part of the image than those of the sequence bands, even though the cold and sequence bands overlap in the LIF spectrum. This separation makes it possible to observe much higher K_a band heads in the rotational contour than was possible in Kirby's room temperature study and, as we show in Sec. III C, to thereby unambiguously determine the rotational constants. Because the differences in the rotational contours arising from the two sets of rotational constants are most apparent at higher J, K_a at the resolution of our laser, the jet-cooled spectrum does not provide a means to separate which set is correct. A further advantage of the 2D-LIF image is that weak rotational transitions that are not apparent in the LIF spectrum are revealed in the rich rotational structure observed. This provides a means for accurate and unambiguous determination of the rotational constants, as we discuss below.

B. Simulating rotational patterns in 2D-LIF images

In a 2D-LIF image of a single vibronic transition, the observed features arise from a series of (absorption, fluorescence) rovibronic transitions. In order to describe a series within the image, we introduce the nomenclature $({}^{\Delta K_a \Delta K_c}\Delta J, {}^{\Delta K_a \Delta K_c}\Delta J)$ to represent a series of related transitions, where the changes in quantum numbers are expressed in the usual P, Q, R notation. A single (absorption, fluorescence) transition pair originating from the $J_{K_a K_c}$ rotational level is denoted as $({}^{\Delta K_a \Delta K_c}\Delta J(J_{K_a K_c}), {}^{\Delta K_a \Delta K_c}\Delta J)$. For example, absorption from the $10_{3,3}$ level in 0_0 to $11_{4,4}$ in 0^0, followed by fluorescence to $10_{5,5}$ in 0_0 would be denoted by the pair

($^{rr}R(10_{3,3})$, ^{pp}R). Note that we follow standard practice, defining the changes in rotational quantum numbers to be the upper value minus the lower value, e.g., $\Delta J = J_{upper} - J_{lower}$. Thus an absorption transition and its identical fluorescence counterpart have the same signs of ΔJ, ΔK_a, and ΔK_c.

In near prolate asymmetric rotors such as fluorobenzene, for a particular J the K states, which are degenerate in the prolate top limit, split. This splitting is largest at low K, leading to the K_a states in the asymmetric top being split at low K_a but near degenerate as K_a approaches J. Looked at from the perspective of how the K_a splitting varies with J for a particular value of K_a, the splitting is unobserved at values where K_a is similar to J but becomes manifest as J increases and the K_a value becomes small compared with J. In the image, there are features that arise from series in J, each series starting with an incremented value of $K_a = J$. The series begins with the two states with the same K_a overlapped but as J increases they split, leading to two separate subseries one where $K_c = J - K_a$ and the other with $K_c = J - K_a + 1$. The subseries with transitions originating from $K_c = J - K_a$ states are referred to as even, whilst the odd subseries comprises transitions originating from $K_c = J - K_a + 1$. When describing the two pairs of degenerate (absorption, fluorescence) transitions we separate the pair with a vertical bar.

To compute images of the rotational structure for comparison with experiment, we first generate a database of all possible transitions from the range of initial rotational states appropriate to the experiment. The image is then computed as follows:

1. The excited state rotational populations produced by the laser at a particular wavelength are calculated. These are determined by where each transition lies within the laser bandwidth, the probability for the transition (i.e., the Hönl London factor), and the initial state population. The laser is assumed to have a Gaussian profile with a full width at half maximum (FWHM) equivalent to the laser linewidth, 0.3 cm^{-1}. Initial state populations were described by a Boltzmann distribution, with appropriate nuclear spin weights. For calculations related to supersonically cooled samples, it was assumed that there is no nuclear spin interconversion during the expansion. Thus for both room temperature and jet cooled samples, the nuclear spin temperature was fixed at the ambient temperature of 295 K. The energy gap in the Boltzmann equation was taken to be the difference in energy between the initial rotational level for the transition and the lowest energy level of the same rotational symmetry.
2. We next determine the emission spectrum from this set of excited rotational levels. Since the fluorescence quantum yield is generally independent of rotational state, the total emission from each excited rotational level is proportional to its population arising from the excitation step. The relative weighting between each of the possible fluorescence transitions from a particular excited rotational state is determined by the Hönl London factors. Emission transitions are assumed to be Gaussian with the linewidth governed by the spectrometer resolution. For the images shown, this was 0.8 cm^{-1}. Note that in doing this we have ignored any changes arising from polarization effects on the fluorescence intensity, which may arise from nonuniform M_J state population distributions associated with the excitation step when a polarized laser is used.[16]
3. Each spectrum calculated as above forms a single line in the calculated image. The complete image is calculated by repeating steps 1 and 2 at each laser wavelength.

The program PGOPHER was used to generate the asymmetric top rotational transitions of fluorobenzene used for the absorption and emission calculations.[17] The energy levels and Hönl London factors were determined using Watson's A-reduced asymmetric top Hamiltonian in representation I^r. J values up to 150 were used and every transition has been included irrespective of absolute intensity. Transitions originating from $J > 150$ are seen weakly in the room temperature 2D-LIF image, however these regions were not used for fitting purposes. Fluorobenzene has a 10:6 ratio for even:odd K_a values due to nuclear spin statistics.

We first simulated a 295 K image of the 0_0^0 transition using the established rotational constants of Kirby.[15] In comparing this image with the experimental image we found that the positions of the calculated features do not reproduce experiment. To illustrate the differences, we have reproduced a small segment of the 2D-LIF image in Fig. 2. The series of vertical features that dominate this image is due to the (^{rr}R, ^{pr}P)|(^{rp}R, ^{pp}P) series. This series has distinct K_a features, where transitions with different initial K_a values are well resolved from each other, allowing observation of the bandheads (this series is fully described in the Appendix). The positions of the bandheads predicted by the rotational constants reported by Kirby are indicated on the figure. In his analysis of the band contour, Kirby noted that there was a second possible set of constants and Fig. 2 also shows the bandhead positions predicted using this set. While Kirby's preferred constants align the features at low excitation energy where his fit was obtained, the fit deteriorates significantly at higher energy. This higher energy region was not visible to Kirby due to overlap from a sequence band but is visible here because the 2D-LIF image separates the two contributions. We find that Kirby's second set of constants provide an improved fit, although the fit also deviates from experiment at higher excitation energy. Not unexpectedly, the image provides a more stringent test for the rotational constants than does a simple 1D contour.

C. Fitting the fluorobenzene origin transition rotational pattern: Determining the rotational constants

Given that the previously accepted rotational constants do not reproduce the image, we have undertaken a fitting process to obtain an improved set. We were interested to establish the precision with which the constants could be determined at the resolution used (0.3 cm^{-1} in absorption; 0.8 cm^{-1} in emission) and to ascertain whether it was possible to observe the effects of higher order terms (centrifugal constants) at this resolution. It transpired that, while we included the known ground state values for the centrifugal constants, we were

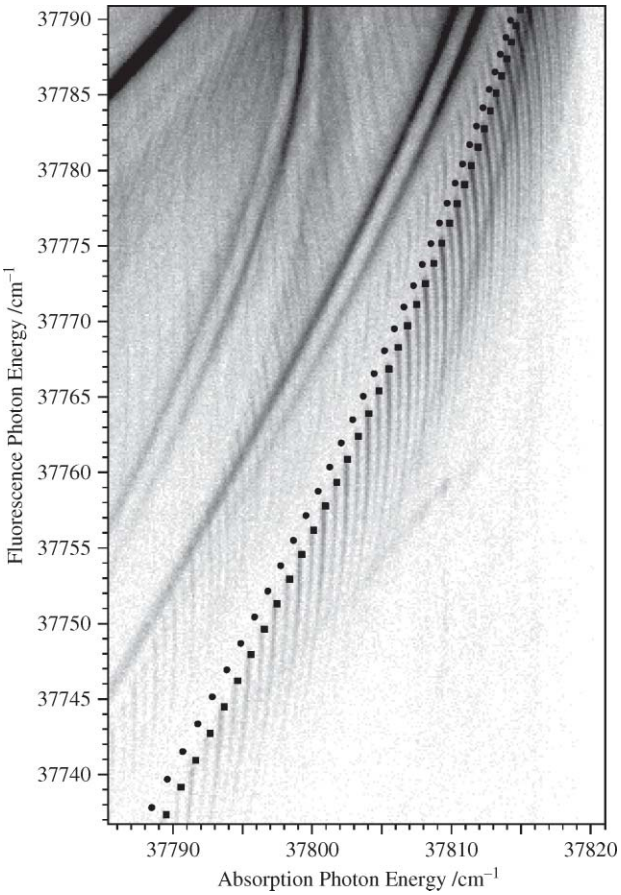

FIG. 2. A segment of the room temperature image shown in Fig. 1 and the position of key bandheads predicted by the constants Kirby reported from his analysis of the rotational contour. Kirby's preferred set of constants give the bandheads shown as filled circles; his second set of constants give the positions indicated by filled squares. The bandheads should align with the top of the vertical features seen. See the text for details.

unable to discern the effects of changes in these constants on the spectrum and retained the S_0 values for S_1.

The fitting process began by varying each of the rotational constants individually to identify features of the 2D-LIF image that were most sensitive to a particular constant. By identifying these features the constants could be individually optimized. Rectangular regions highlighted in Fig. 3 show examples of features in the image that were used to optimize each of the rotational constants (these features are discussed in detail in the Appendix). The fitting process focused on fitting the positions of these features and subsequently checking the accuracy of the complete image. For each feature of the image used to determine a particular constant, many positions along that feature were used to determine a value for the rotational constant under consideration. The minimum number of points used was 36, when deducing the ΔA value. The appropriate rotational constant was iteratively varied to move each calculated position through that on the observed image, with the best fit at that point determined by the maximum overlap, i.e., minimized energy difference. This provides a value for the constant at each of the points chosen. We report the average and standard deviation of these individual determinations when presenting the values for each rotational constant.

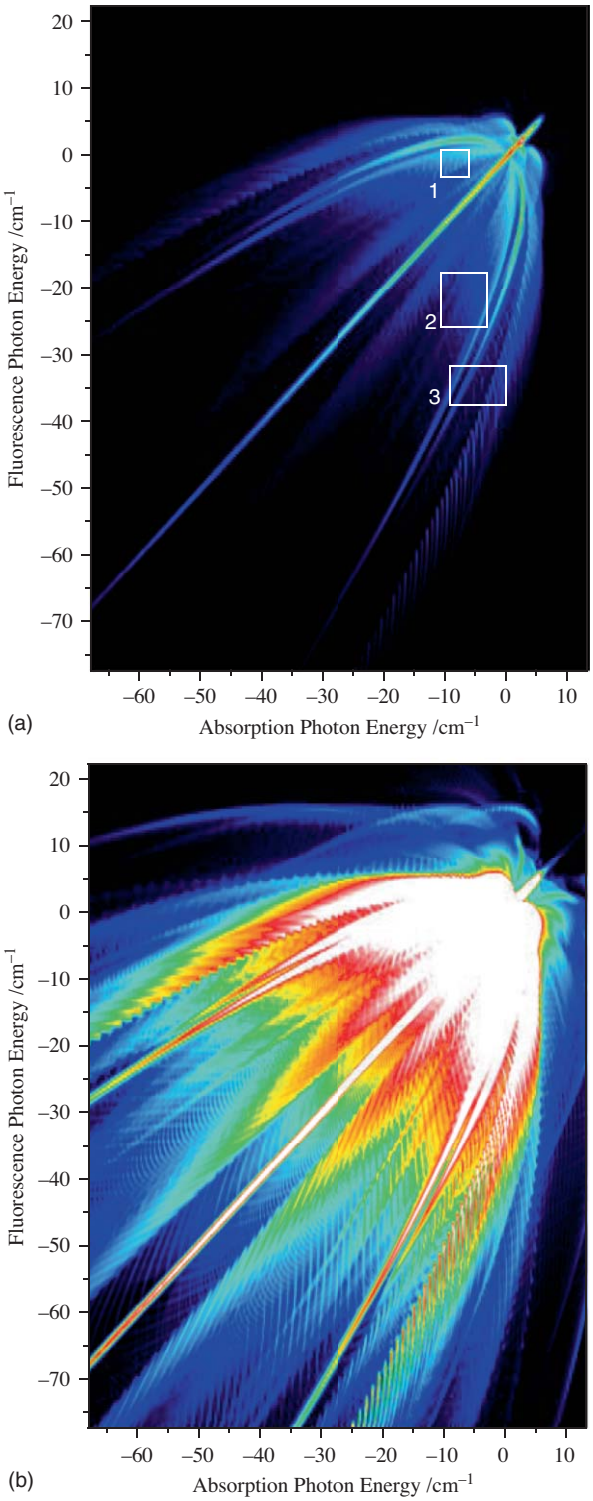

FIG. 3. The calculated image of the rotational structure associated with the 0_0^0 band using our final set of rotational constants. The intensity is displayed on a logarithmic scale. (a) and (b) show the same image, but the intensity scale has been magnified in (b) to highlight weaker features. Rectangular sections are highlighted to show features used to determine each of the rotational constants. See the Appendix for details.

Using the different series and image segments discussed in the Appendix, values of ΔA, ΔC, and ΔB were determined in that order. The process was iterated several times until convergence was achieved. The final calculated image is shown in Fig. 3 and an animated GIF file comparing the

TABLE II. Experimental rotational constants of fluorobenzene.

		S_1 Excited state		
Constant	S_0 Ground state[a]	Kirby[b] preferred	Kirby[b] alternative	This work
A /cm^{-1}	0.18892115	0.1777	0.1784	0.178315(3)
B /cm^{-1}	0.08574776	0.08474	0.08459	0.084713(7)
C /cm^{-1}	0.05897125	0.05738	0.05738	0.057421(5)
Δ_J /cm^{-1}	4.4425×10^{-9}			[c]
Δ_{JK} /cm^{-1}	7.150×10^{-9}			[c]
Δ_K /cm^{-1}	2.790×10^{-8}			[c]
δ_J /cm^{-1}	1.453×10^{-9}			[c]
δ_K /cm^{-1}	1.2442×10^{-8}			[c]
Δ[d] /amu.Å^2	0.035232	0	0	0.04(3)
κ[e]	−0.587895	−0.545	−0.550	−0.5485(1)

[a]Values for the 0_0 level determined from Kisiel *et al.*'s microwave study (Ref. 14).
[b]Preferred values are those tabulated by Kirby, while the alternative values are determined from his second choice of ΔA, assuming the inertial defect to be zero (Ref. 15).
[c]Ground state higher order terms were used for the excited state.
[d]$\Delta = I_c - I_a - I_b$.
[e]$\kappa = (2B - A - C) / (A - C)$.

calculated and observed images is supplied as supplementary information.[18] The rotational constants determined are given in Table II. This table includes the S_0 values determined by microwave techniques and Kirby's two sets for S_1. It is interesting to note the additional precision with which we have been able to determine the constants, in spite of our lower resolution compared with Kirby. This arises because we are able to observe much higher J, K_a states due to the 2D-LIF method disentangling overlapping sequence structure. Fitting different features of the 2D-LIF image to different constants has the advantage that it is not necessary to assume that the molecule remains planar in the excited state. This is in contrast to most band contour analyses of aromatic compounds where the assumption of planarity is necessary and allows only two rotational constants to be fitted to the experimental spectrum, with the third constant determined assuming the inertial defect is zero. An interesting feature of the 2D-LIF image is the extent to which it reveals weak features that are unobservable in the LIF spectrum, for example, series arising from $\Delta K_a = \pm 3$.

Comparing our values with those of Kirby reveals interesting differences. Our best fit value of ΔA was determined to be $-0.010606(3)$ cm^{-1}, >5% different from Kirby's preferred choice of $\Delta A = -0.0112$ cm^{-1} and ~1% different from his alternate choice of $\Delta A = -0.0105$ cm^{-1}. Kirby assigned the strong:weak intensity alternating features between -2 and -12 cm^{-1} to bandheads of the ^{pr}Q series and from this determined $\Delta A = -0.0112$ cm^{-1}. However, the peak separation between the dominant peak in the spectrum and the weaker peak to higher energy suggested an alternative value of $\Delta A = -0.0105$ cm^{-1} which, for a number of reasons, was rejected. Using our fitted constants we are now in a position to identify the origin of this discrepancy. We find that two $^{\Delta K_a}\Delta J$ series show significant K_a structure in this region. By computing and comparing absorption spectra for these two series individually, the series responsible for each feature in the absorption spectrum can be identified. These spectra are shown in Fig. 4. In the region -2 to -10 cm^{-1} the peaks seen in the two series overlap, with the intensity of the ^{rr}R|^{rp}R peaks being more than twice those of the ^{pr}Q series. To lower the energy the peak positions in the two series diverge. Kirby gave preference to the $\Delta A = -0.0112$ cm^{-1} value because spectra calculated using $\Delta A = -0.0105$ cm^{-1} displayed the wrong divergence for the ^{pr}Q series, which he believed was primarily responsible for the observed structure. His preferred constants are incorrect because the features were assigned to the wrong series: the series with the largest contribution to the K_a band heads is ^{rr}R|^{rp}R.

The $\Delta C = -0.001550(5)$ cm^{-1} rotational constant determined in this work compares very well to Kirby's value of $\Delta C = -0.00158(2)$ cm^{-1}. The agreement is reassuring since Kirby determined the value by fitting ^{rp}P|^{pp}P transitions to fine structure observed in the absorption spectrum, whereas our value was extracted by fitting to the shape of the (^{rr}R, ^{rp}P)|(^{pr}R, ^{pp}P) two-dimensional sequence. It is common in band contour analyses to assume that ΔB can be derived for planar molecules by setting the inertial defect, Δ, to zero,

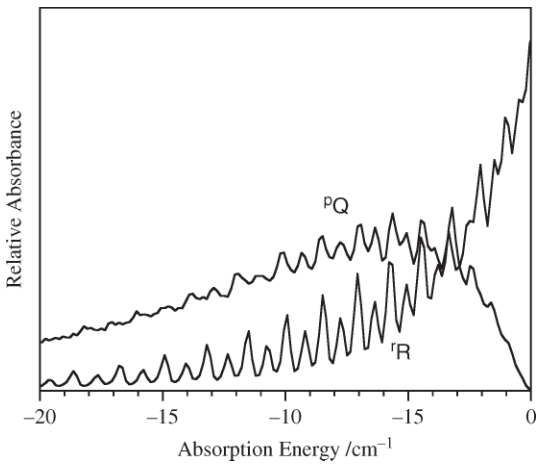

FIG. 4. A comparison of absorption spectra for each $^{\Delta K_a}\Delta J$ series individually to identify the series responsible for each feature in the absorption spectrum. The features are dominated by ^{r}R (consisting of the ^{rr}R|^{rp}R transitions) rather than the ^{p}Q assigned by Kirby. In the region -2 to -10 cm^{-1} the two series overlap, but the intensity of ^{r}R is more than twice that of the ^{p}Q series. To lower energy the peak positions in the two series diverge.

where $\Delta = I_c - I_a - I_b$ and Kirby used this approach. Analysis of the 2D-LIF image provides a direct measure of ΔB, which was found to be $\Delta B = -0.001035(7)$ cm^{-1}. This results in a slightly positive (albeit with a large standard deviation) inertial defect of 0.04(3) amu Å^2. This value is similar to that determined for S_0.

Recently, *ab initio* calculations have been reported for S_0 and S_1 fluorobenzene at a number of levels of theory.[13] Using the S_0 and S_1 geometries determined at each level of theory, we have computed the rotational constants to compare with those we have obtained. This allows us to identify the level of theory that provides the geometry that most closely matches experiment and to determine how accurate the match is. Using the PMIFST program,[19] rotational constants were determined from the *ab initio* geometries calculated at each of the levels of theory. These are shown in Table III. A figure of merit can be defined by the sum of the squares of the differences between the experimental and calculated values, expressed as a fraction of the experimental value, for each rotational constant. On this basis, the geometry that provides the best match with our constants comes from the CCSD/6–311G** calculations, although there is little advantage over the less computationally expensive RI-CC2/def2-TZVPP calculations. CCSD and CC2 are of comparable quality, both being based on the coupled cluster approach to treating electron correlation; however, RICC2 is computationally more efficient due to its resolution of the identity (RI) treatment allowing accurate calculations for larger molecules.[20]

The remaining spectroscopic constant derived from the experimental image is the location of the band origin. From our fitting of the rotational contour of both the room temperature and jet cooled spectra (see Sec. IV for details of the cold spectrum), we determine the band origin of the 0_0^0 transition to be located at 37 813.8 ± 0.1 cm^{-1}. This is consistent with other origin determinations by Kirby (37 813.9 ± 0.1 cm^{-1})[15] and Butler *et al.* (37 813 cm^{-1}).[12] The intense central peak in the room temperature absorption spectrum is blue shifted from the origin by 2.2 cm^{-1} (i.e., it is at 37 816.0 ± 0.1 cm^{-1}), which is in excellent agreement with Lipp and Seliskar's value of 37 816.2 cm^{-1}.[9,10]

D. Vibrational structure and the spectral manifestation of Fermi resonance in 2D-LIF: The role of off-diagonal features

Butler *et al.* noted that the S_1–S_0 fluorobenzene spectrum is littered with Fermi resonances.[12] The 2D-LIF technique provides a means to identify bands connected by Fermi resonance. Where two zero-order states, one of which is "dark," $|\phi_D\rangle$, and the other "bright," $|\phi_B\rangle$, interact via Fermi resonance, the two resulting states, $|\psi_1\rangle$ and $|\psi_2\rangle$, are linear combinations of the zero order states:

$$|\psi_1\rangle = a\,|\phi_B\rangle + b\,|\phi_D\rangle$$

$$|\psi_2\rangle = -b\,|\phi_B\rangle + a\,|\phi_D\rangle$$

and both states are seen in the spectrum due to their having a component of $|\phi_B\rangle$.

TABLE III. Computational rotational constants of fluorobenzene.[a]

	RI-CC2/def2-TZVPP			RI-CC2/aug-cc-pVDZ			CCSD/6-311G**			SACCI/6-311G**			TDDFT/B3-lyp/def2-TZVPP		
Constant	S_0	S_1	Δ[b]	S_0	S_1	Δ	S_0	S_1	Δ	S_0	S_1	Δ	S_0	S_1	Δ
A /cm^{-1}	0.19010	0.17860	−0.01150	0.18573	0.17471	−0.01102	0.18906	0.17876	−0.01031	0.19079	0.18249	−0.00830	0.19035	0.17998	−0.01037
B /cm^{-1}	0.08576	0.08492	−0.00083	0.08395	0.08323	−0.00072	0.08553	0.08439	−0.00114	0.08580	0.08478	−0.00102	0.08587	0.08550	−0.00036
C /cm^{-1}	0.05910	0.05756	−0.00154	0.05782	0.05637	−0.00144	0.05889	0.05733	−0.00156	0.05919	0.05789	−0.00130	0.05917	0.05796	−0.00121
Figure of Merit[c]	0.058×10^{-3}		0.046	2.152×10^{-3}		0.097	0.033×10^{-3}		0.011	0.727×10^{-3}		0.074	0.334×10^{-3}		0.471

[a]Rotational constants calculated using the geometries computed by Pugliesi *et al.* (Ref. 13)
[b]$\Delta = S_1 - S_0$.
[c]Figure of merit $= \Sigma[(V_{calc} - V_{expt})/V_{expt}]^2$ where V_{calc} is a calculated value and V_{expt} is the corresponding experimental value. Figures of merit are calculated separately for the absolute rotational constants and the change in rotational constants between S_1 and S_0. A good agreement between calculated and experimental values is demonstrated by a low figure of merit.

Where the Fermi resonance occurs in the excited electronic state, the 2D-LIF pattern will involve two bands on the image diagonal, corresponding to the transitions from the 0_0 level to each of the two states and a series of bands along the fluorescence (vertical) axis to lower energies. The fluorescence axis will show transitions due to both the $|\phi_B\rangle$ and $|\phi_D\rangle$ components in the emitting levels. A similar pattern can occur when two nearby transitions are allowed and a Fermi resonance interaction is absent. As is usually the case, the key to identifying a Fermi resonance is the presence of bands with unexpectedly high intensity. Because the S_1 and S_0 vibrational frequencies can change significantly, the particular features observed experimentally will depend on the fluorescence region monitored.

For S_0 resonances observed through hot or sequence bands a different pattern emerges, and hence S_0 and S_1 resonances are readily distinguished. The transitions form a "square" pattern on the image with sides of ΔE, the energy separation between the two Fermi resonance states. The features on the image diagonal have an intensity ratio of a^4:b^4 while the off-diagonal features have intensity a^2b^2. Because Fermi resonances often involve close-lying states, provided the laser and fluorescence windows encompass the same wavelength region, the complete pattern will be seen. The off-diagonal features arise from fluorescence transitions that terminate in the other Fermi resonance level rather than the one initially excited from. As for the S_1 resonance case, a similar pattern is produced for allowed transitions in the absence of Fermi resonance, and it is intensity anomalies that identify the situation as a Fermi resonance. We have identified two patterns in the room temperature scan of the origin region that might arise from S_0 Fermi resonances.

The first pattern of this kind observed in Fig. 1 involves the pair of sequence bands at 37 780.8 cm^{-1} and 37 783.5 cm^{-1} (shifted -35.2 cm^{-1} and -32.5 cm^{-1} from the 0_0^0 band, respectively). Interestingly, these bands were not listed by Lipp and Seliskar in their report of the hot band and sequence structure in fluorobenzene, although they report a very weak band at 37 786.4 cm^{-1} (a shift of -29.8 cm^{-1} from the 0_0^0 band).[10] Figure 5(a) shows an enlargement of this region of the image. The two features off the image diagonal are observed while the features on the image diagonal are obscured by the intensity of the 0_0^0 image diagonal. Figure 5(b) shows the transitions responsible for the features on an energy level diagram. Based on the S_0 and S_1 frequencies reported by Butler *et al.*,[12] we assign these two bands to a Fermi resonance involving 10_1 and 30_2. From the S_1 frequencies, we suggest that the transitions seen have oscillator strength through the 30_2^2 component. Evidence for 10_1 being involved in a Fermi resonance comes from the IR spectrum reported by Lipp and Seliskar.[21] These authors report the ν_{10} band (ν_{12} in the Wilson's notation they used) to show a split Q branch, with the two peaks at 807.3 and 810.1 cm^{-1}. They did not provide a rationale for this observation. The 2.8 cm^{-1} splitting observed by Lipp and Seliskar closely matches our 2.7 cm^{-1} measurement.

In order to confirm this S_0 resonance we have measured two 2D-LIF images (not shown) to compare the relative intensity of 30_0^2 and 30_2^0. These images were measured using a supersonic free jet cooled sample to contract the rotational contours. The first image was recorded by scanning the laser over the $10_0^1 \cdots 18_0^1 19_0^1$ Fermi resonance pair while monitoring the $10_1^1/30_2^2$ region in dispersed fluorescence. The notation $10^1 \cdots 18^1 19^1$, introduced by Butler *et al.*,[12] refers to a Fermi level arising from interaction between 10^1 and $18^1 19^1$, where the first vibrational mode specified, 10^1 in this case, has the larger contribution in the mixed state. This image allows us to extract the intrinsic relative intensity of 30_0^2 compared with 10_0^1. 30_0^2 was not seen in the LIF spectrum by Butler *et al.* but is expected to appear between the two intense bands associated with the $10_0^1 \cdots 18_0^1 19_0^1$ Fermi resonance pair. We observe it in the 2D-LIF image at an excitation of $0_0^0 + 775.9$ cm^{-1} via observation of the 30_2^2

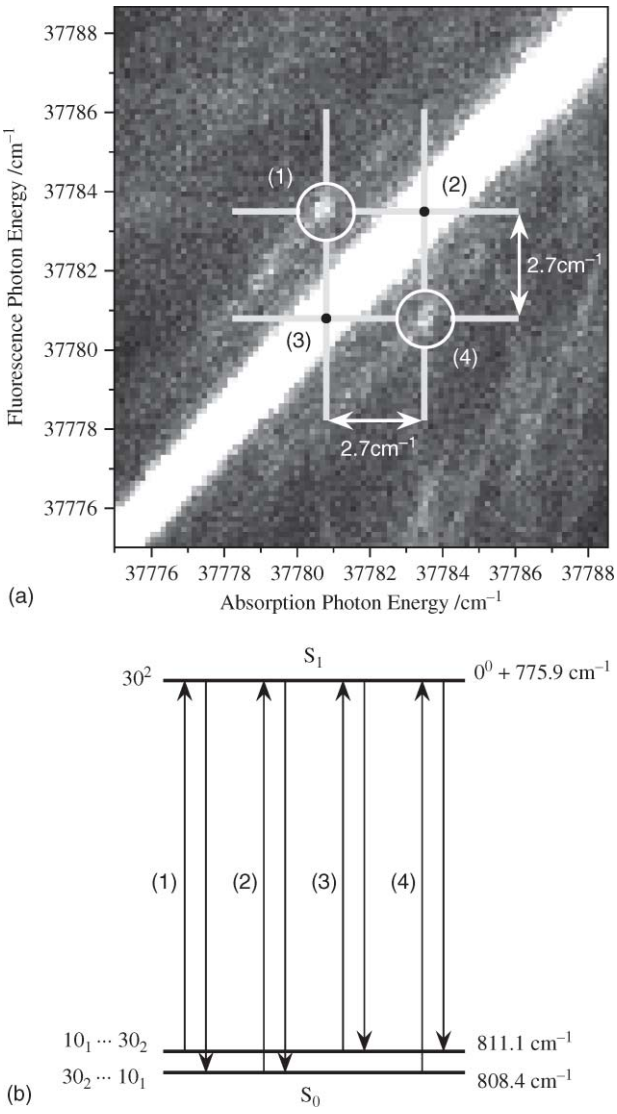

FIG. 5. (a) An enlargement of the region of Fig. 1 that contains the sequence bands at 37 780.8 cm^{-1} and 37 783.5 cm^{-1} (shifted -35.2 cm^{-1} and -32.5 cm^{-1} from the 0_0^0 band, respectively). This region shows the pattern expected for a Fermi resonance, and the relevant features are highlighted in the figure. We assign the pattern to transitions between the $10_1/30_2$ Fermi resonance pair and 30^2. The intensity is displayed on a linear gray scale, which provides the best contrast for observing the weak features. (b) An energy level diagram displaying transitions between the $10_1/30_2$ Fermi resonance pair and 30^2. The four (absorption, fluorescence) transitions are labeled and correspond with the points identified in (a).

fluorescence band. The 30_0^2 band is measured to have 3% of the combined intensity of the two Fermi resonance bands (which have the 10_0^1 intensity split between them). Assuming the same intensity ratio for the analogous transitions from 0^0, 10_1^0 is expected to have ca. 34 times the intensity of 30_2^0. The second 2D-LIF image involved scanning the laser over the 0_0^0 band region while the dispersed fluorescence monitored the $10_1^0/30_2^0$ band region. 30_2^0 has significantly higher intensity than expected (55% of the intensity of 10_1^0) confirming the S_0 Fermi resonance between 10_1 and 30_2.

The unperturbed frequencies and the interaction matrix element, V, can be determined from the intensities and band positions extracted from the second of the images discussed above. We measure the Fermi pair at S_0 frequencies of 808.4 and 811.1 cm^{-1}. These values are different from the Q branch positions reported by Lipp and Seliskar by 1 cm^{-1}.[21] We calculate the unperturbed frequencies to be $10_1 = 810.2$ cm^{-1} and $30_2 = 809.4$ cm^{-1} while $V = 1.3$ cm^{-1}. Butler *et al.* have noted that the 14_2^0 transition is more intense than expected and speculate that this may be due to a Fermi resonance involving 14_2 and 10_1. This has not been included in our calculations, which treat the local $10_1/30_2$ interaction as a simple two level situation.

This assignment leads to the prediction of other sequence bands from this Fermi resonance that should occur in the region observed. As noted above, 10^1 is involved in a Fermi resonance with 18^119^1 in the S_1 state. 30^2, while it lies in the region of this excited state Fermi resonance, is not believed to be involved in the S_1 resonance.[12] As a result, three sets of sequence band pairs should be present in the image, along with the corresponding off-diagonal features, corresponding to transitions from the $10_1/30_2$ Fermi pair to $10^1\cdots18^119^1$, 30^2 and $18^119^1\cdots10^1$. These sequence pairs are centred at −43.5, −33.9, and −27.1 cm^{-1}, respectively. From the relative intensities seen for the $10^1\cdots18^119^1$ Fermi resonance pair, we have determined the relative intensity pattern for the 12 transitions predicted to arise in the 2D-LIF image. This analysis reveals that the other features will be substantially weaker (by a factor of 5 or more) relative to the features centred at −33.9 cm^{-1}, which explains why they are not seen. In this context we note the very weak band at a shift of −29.8 cm^{-1} reported by Lipp and Seliskar.[10] We suggest that this is the transition from the upper $10_1\cdots30_2$ level to the $18^119^1\cdots10^1$ level, which is one of the more intense of the additional features expected. It is predicted to occur at −28.5 cm^{-1}. Rademann *et al*. have reported a number of sequence bands of fluorobenzene as a part of their study of the fluorobenzene-Ar complex.[6] While the sequence bands are of low intensity and generally broad, making precise band positions difficult to determine, their reported bands at 33.8 and 44.4 cm^{-1} are consistent with our analysis.

The second Fermi resonance pattern seen in the 2D-LIF image in Fig. 1 is interesting because it involves a long range interaction that is unlikely to be recognized as a Fermi resonance were it not for the observed off-diagonal pattern. We see off-diagonal features at (37 809.5, 37 758.9) and the mirror position (37 758.9, 37 809.5), which connect the two levels 11_1 and 20_2. In this detection region the corresponding image diagonal features are notionally due to $11_0^120_2^0$ or 11_1^1 in both absorption and emission while the off-diagonal features are due to $11_0^120_2^0$ in absorption and 11_1^1 in emission, and vice versa. Butler's spectra show 20_2^0 to be quite weak and 11_0^1 to have negligible intensity.[12] Therefore the $11_0^120_2^0$ transition is not expected to be seen. The presence of the off-diagonal features suggests that "20_2" is a mixed state and in this region is deriving intensity from the 11_1^1 transition through having a component of 11_1. We place a caveat on this rationale to the extent that, while Butler *et al.* do not see 11_0^1 in their LIF spectrum, they do assign a reasonably strong band in the 0^0 DF spectrum to 11_1^0. The reason why these related transitions have apparently quite different intensities has not been explained. Interestingly, we note that 11_0^1 is observed as a very weak feature in the absorption spectrum of Lipp and Seliskar[3] and in the REMPI spectrum reported recently by Pugliesi *et al.* (labeled $6a_0^1$ in the Wilson's notation they used).[13]

IV. SUPERSONIC FREE JET SPECTRA

The sensitivity displayed in the room temperature 2D-LIF image led us to explore the sensitivity of the technique further. Resonance enhanced multiphoton ionisation, in combination with mass detection, has been used to identify features in the S_1–S_0 spectrum due to different isotopic variants and we explore the extent to which the high resolution 2D-LIF spectrum can provide a means to assign features to these different species in a supersonic expansion.

A. Supersonic free-jet spectrum

Figure 6 shows a 2D-LIF image of fluorobenzene cooled in a supersonic free jet expansion of argon, recorded in the region of the origin band. The dominant feature is the 0_0^0 band at (37 813.8 cm^{-1}, 37 813.8 cm^{-1}). The mirror symmetry that was evident in the rotational structure about the image diagonal in the room temperature case is less apparent in the free jet image because the narrower rotational level population distribution leads to more obvious asymmetry in intensity between features that arise from low energy levels and end in higher ones versus the reverse process. Along the fluorescence axis one can see a series of very weak features above and below the 0_0^0 band. These are due to grating ghosts, visible because of the high intensity of 0_0^0 in this image. A weak feature with the same characteristic fluorobenzene shape is seen on the image diagonal 4.0 cm^{-1} to the blue of 0_0^0. We assign this to the 0_0^0 band of $^{13}C^{12}C_5H_5F$ arising from the natural abundance of ^{13}C in the fluorobenzene sample. The characteristic fluorobenzene rotational pattern makes identifying this as a separate feature straightforward. The spectral structure from ^{13}C isotopomers is discussed further in Sec. IV B. A further band, clearly assignable to fluorobenzene based on the rotational pattern, is seen at (37 797.1 cm^{-1}, 37 797.1 cm^{-1}), i.e., 16.7 cm^{-1} to lower laser wavenumber. This is assigned to the sequence band 30_1^1 and arises from incomplete vibrational cooling in the expansion. This band is also seen in the room temperature image (Fig. 1).

In the region 30–40 cm^{-1} to the blue of the fluorobenzene origin band we observe three very weak overlapping

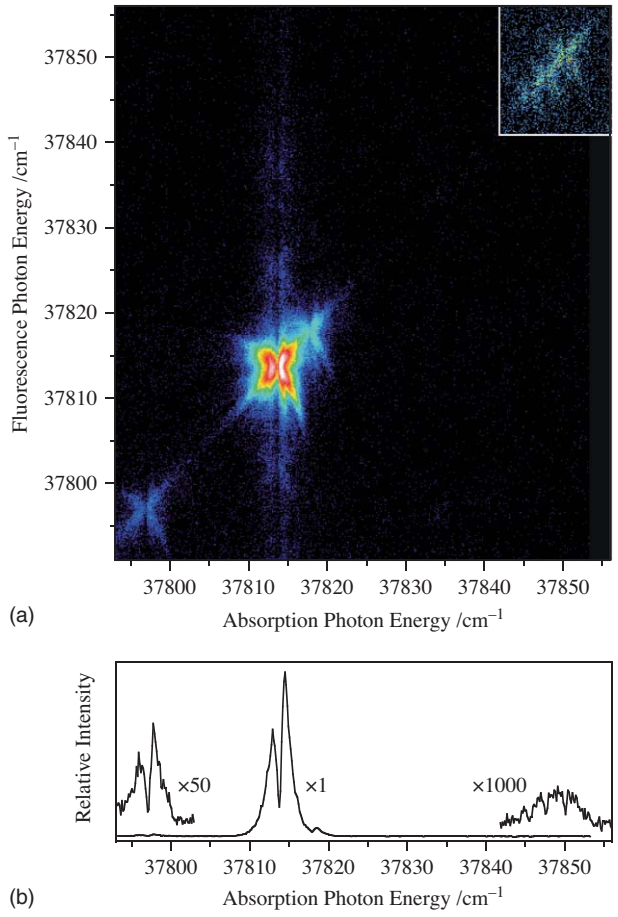

FIG. 6. (a) 2D-LIF image of a supersonically cooled sample of fluorobenzene. The laser is scanned in the region of the 0_0^0 transition while the spectrometer is set to detect fluorescence in the same region. The intensity is displayed on a logarithmic scale. The lower panel, (b), shows the laser induced fluorescence (LIF) spectrum generated by projecting the 2D-LIF image onto the laser (absorption) axis.

absorption bands whose rotational structure is consistent with them arising from fluorobenzene. Based on the previously reported spectrum of *p*-deuterofluorobenzene,[9,10,22] we assign these to the 0_0^0 transitions of different isotopomers of fluorobenzene-d_1 present at natural abundance, as discussed below.

B. Spectral features from isotopes in natural abundance

The three overlapping transitions observed at 36.3, 33.9, and 31.8 cm^{-1} to the blue of the fluorobenzene 0_0^0 transition are assigned to monodeuterated fluorobenzene in natural abundance. Three bands arise because the deuterium can substitute at the *ortho*, *meta*, or *para* positions relative to the fluorine atom giving three isotopomers. The ratio of *ortho:meta:para* is 2:2:1 because of the number of possible positions for the deuterium. It can be seen that the lower energy band is weaker than the other two, which are of similar intensity. Consequently, we assign it to the *para* species. There have been several previous spectroscopic studies reported for the *para* species.[9,10,22] The origin band of *para*-fluorobenzene-d_1 is reported in these studies to be blue shifted from the fluorobenzene 0_0^0 band by 31.9 and 32 cm^{-1}. Our analysis gives a value for the shift of 31.8 cm^{-1}, in excellent agreement. There have been no reports of S_1–S_0 spectra for the *ortho* or *meta* isotopomers. To see if the two isotopomers might have sufficiently different rotational contours to separate them by this means, we simulated the contours using rotational constants based on the CCSD/6–311G** geometries (see Sec. III C). It was found that at the resolution and signal to noise of our data, the small changes to the contour predicted would not be observable. Thus we are unable to distinguish which of the remaining two bands is *ortho* and which is *meta*. The combined intensity of these monodeuterated fluorobenzene bands relative to the fluorobenzene origin band is 0.041%. Since there are five sites for deuteration, this corresponds to an isotopic abundance for deuterium of 0.0082% which is within the range of natural variability.[23]

The absorption shift due to ^{13}C is considerably smaller than that seen for deuteration. The image for the supersonically cooled sample (Fig. 6) shows a feature blue shifted in absorption and fluorescence by 4.0 cm^{-1} that we assign to the origin band of ^{13}C isotopomers. As noted above, Dimopoulou-Rademann *et al.* reported the ^{13}C shift as 1.9 cm^{-1}.[24] We ascribe the differing values to the different resolutions of the laser systems used in the two experiments. Interestingly, due to substitution in different positions, fluorobenzene containing a single ^{13}C should in principal show several origin band positions analogous to what is seen for the deuterated species. Four bands are expected, with an intensity ratio of 1:2:2:1, due to ^{13}C at the *ipso*, *ortho*, *meta*, and *para* positions, respectively. Of course, based on the similarity of the shifts seen for the three deuterated isotopomers, we would expect the separation between the different isotopomer origin bands to be small given the much smaller shifts involved. The problem with distinguishing multiple ^{13}C frequency shifts while monitoring the 0_0^0 band in both absorption and emission is that the transitions appear on the diagonal, with the large ^{12}C intensity dominating and obscuring any additional ^{13}C transitions. To see whether we could separate the ^{13}C isotopomers, we measured a 2D-LIF image with the laser scanned over the 0_0^0 band region while the 11_1^0 band region was monitored in dispersed fluorescence, this emission being in a region with cleanly separated bands.[12] Monitoring a region where the transition terminates in a vibrational level (rather than the zero point level, as was the case with 0_0^0) introduces the possibility that the vibrational frequency change will move the ^{13}C vibrational frequencies further from the ^{12}C bands and hence separate these bands better in the emission step. Figure 7 shows the resulting 2D-LIF image.

This image shows three features. The strong ^{12}C feature at (37 813.8, 37 297.5) is accompanied by a weak ^{13}C feature at (37 817.8, 37 302.8), corresponding to the 4.0 cm^{-1} separation expected. However, a third, very weak feature is seen at (37 816.8, 37 305.1), corresponding to an absorption frequency shift of 3.0 cm^{-1}, which we assign to a different ^{13}C isotopomer. It is visible because it is blue shifted in fluorescence further than the more intense ^{13}C feature. Analysis of the relative intensities of the two ^{13}C bands reveals an intensity ratio of ~5:1 implying that three of the four isotopomers have an essentially identical shift at our

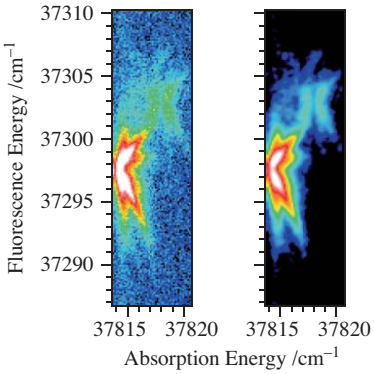

FIG. 7. 2D-LIF image of a supersonically cooled sample of fluorobenzene with the laser scanned in the region of the 0_0^0 transition and the spectrometer set to detect fluorescence in the region of the 11_1^0 band. The left-hand image displays the unaltered experimental image, whilst the right-hand image has been convoluted with a 2D Gaussian function to visually enhance the weak ^{13}C features. Only the high energy side of the intense ^{12}C band is visible in the image. The intensity is displayed on a logarithmic scale.

resolution and that either the *ipso* or the *para* ^{13}C substitution produces a smaller 0_0^0 shift compared to the other isotopomers. We suggest that the *ipso* isotopomer has the reduced shift, our reasoning being that (i) when the ^{13}C is attached to F, the change in reduced mass for the CF "group" is less than is the case for CH, leading to smaller vibrational frequency changes, and (ii) in the case of deuteration, the shift for *para* is very similar to those for *ortho* and *meta*, suggesting that the same is likely to be the case for ^{13}C substitution.

This study of isotopomers shows the advantage of adding the second energy dimension in the 2D-LIF approach. 2D-LIF is able to distinguish features from isotopomers of the same mass that a mass-based detection scheme such as mass resolved REMPI would reveal as a series of overlapped bands.

V. REQUIREMENTS FOR IMPLEMENTATION OF HIGH RESOLUTION 2D-LIF

Having demonstrated that 2D-LIF imaging can be a powerful technique for observing and analyzing polyatomic rovibronic spectra, in this section we address the issue of how readily the apparatus for undertaking these experiments can be put together. The photon detection side is straightforward: image intensifiers with sufficient amplification for single photon detection are readily available, as are CCD cameras. Alternatively, high sensitivity 2D photon detection systems are commercially available. Our implementation of the technique is based on a home built spectrometer with reasonable dispersion (ca. 5 cm^{-1} per mm in the region of interest), and the images we have reported have used a spectrometer resolution of 0.8 cm^{-1}. The key for the technique to be straightforwardly implemented is the availability of commercial spectrometers of sufficient resolution. Spectrometers capable of achieving a resolution of 2 cm^{-1} are available from several suppliers. This is somewhat below the resolution that we have shown in the fluorobenzene study; however, it is sufficient for much of the rotational structure to be revealed and distinguished from overlapping sequence bands. This is particularly so when the rotational structure leads to band heads separable in the laser

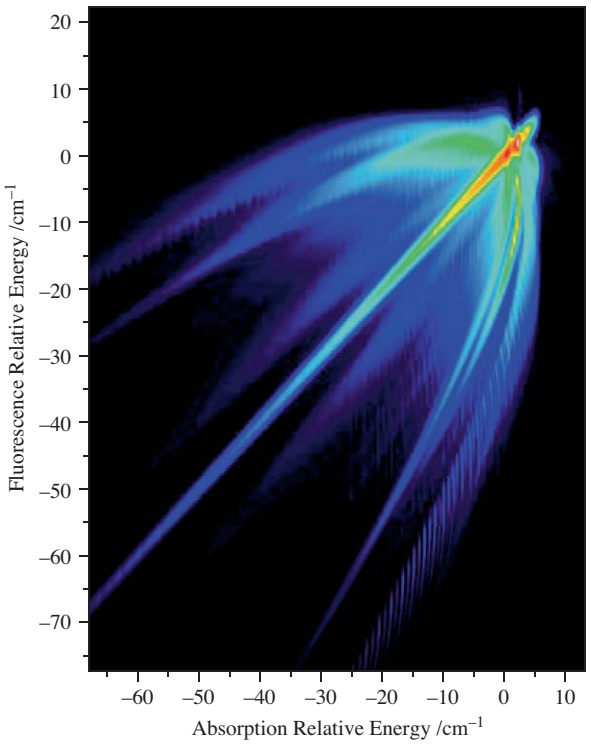

FIG. 8. As for Fig. 4(a) but with the fluorescence resolution degraded to 2.0 cm^{-1} to illustrate what can be achieved with commercially available spectrometers.

axis, which is a regular situation for aromatics, as discussed by Kirby.[25] To illustrate the image that is expected for an experiment based on a commercial spectrometer, we show in Fig. 8 an image calculated with the laser resolution unchanged and the fluorescence resolution reduced to 2 cm^{-1}. Comparing this with the image calculated for our 0.8 cm^{-1} fluorescence resolution, Fig. 3, it can be seen that, while there is a blurring of features, which is particularly evident for features above the image diagonal, significant detail remains. In particular, K_a band structure separated on the laser axis is clearly observed in features below the image diagonal. This indicates that the 2D-LIF imaging technique can be performed with "rotational resolution" using commercially available instrumentation.

The excitation step in our experiments was performed using a standard commercial dye laser operating without an etalon. In considering resolution issues, we have also explored the gains that might be made by using a narrower linewidth laser source. It transpires that there are some advantages although, since overlapped features are already teased apart to a significant extent, they are likely to be of most benefit for larger molecules where the 2D-LIF image fails to separate structure at the lower laser resolution.

VI. CONCLUSIONS

We have illustrated a high resolution 2D fluorescence technique, which we refer to as two- dimensional laser induced fluorescence imaging, for measuring images of rovibronic transitions for polyatomic molecules from which one can extract rotational constants. The technique involves

scanning a tunable laser over absorption features in the S_1–S_0 electronic spectrum while monitoring a segment of the dispersed fluorescence spectrum. Because of the combination of the size of the image intensifier we use and the dispersion of our spectrometer, we have monitored a 100 cm^{-1} wide segment. The technique has been illustrated by application to the S_1–S_0 transition in fluorobenzene. 2D-LIF imaging allows features that overlap in the usual LIF spectrum to be separated. We have shown that the overlap of rotational contours by sequence band structure can be significantly reduced with 2D-LIF allowing a much larger range of rotational transitions to be observed and higher precision rotational constants to be extracted. The rotational constants that we have determined for S_1 fluorobenzene are an order of magnitude more precise than those extracted previously from the rotational contour. The previously determined values were found to be in error by as much as 5%. A significant advantage of 2D imaging is that it separates the rotational contours into constituent branches that can be targeted to determine the three rotational constants without the need for approximations such as that of planarity. 2D-LIF imaging has been shown to be a sensitive method capable of detecting weak spectral features, particularly those that are otherwise hidden beneath stronger bands. Two ground state Fermi resonances were identified by the patterns that such resonances produce in the images. With the use of an image intensifier working at the single photon detection limit, 2D-LIF imaging is a sensitive technique. The sensitivity of the technique was demonstrated by our observation of the three isotopomers of fluorobenzene-d_1 in natural abundance in an image taken of a supersonically cooled sample. The ability to separate some of the ^{13}C isotopomers in natural abundance was also demonstrated. The equipment required to perform 2D-LIF imaging at "rotational resolution" is available from commercial suppliers.

ACKNOWLEDGMENTS

We wish to acknowledge and thank Dr. Colin Western of University of Bristol for providing a Command line version of his PGOPHER program and Dr. Martin Cockett from the University of York for supplying information concerning his group's *ab initio* calculations for fluorobenzene. We thank the School's Electronic and Mechanical workshop staff for their support in constructing and maintaining the apparatus. This research was supported by the Australian Research Council and Flinders University.

APPENDIX: DETAILS OF THE ROTATIONAL ANALYSIS

This Appendix gives details of the rotational features used to determine the rotational constants for the 0^0 level of S_1 fluorobenzene. The three principal constants A, B, and C were determined. Because of their intertwined influence on features of the image, they were determined in the order A, C, B. The spectra are primarily sensitive to the differences between the ground and excited state rotational constants, and hence we refer to the determination of these differences in the discussion below. The excited state constants are then calculated from the well-determined ground state values.

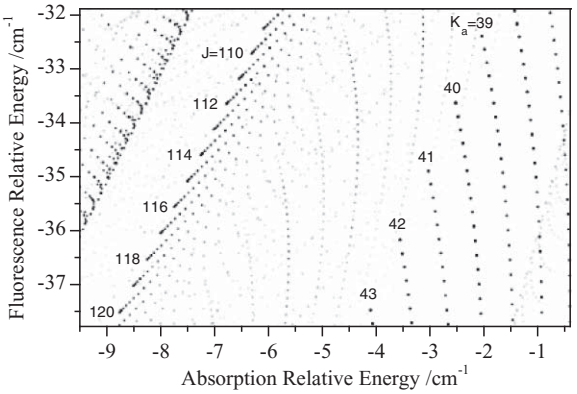

FIG. 9. 2D-LIF image of fluorobenzene calculated at room temperature with a very high resolution (FWHM of 0.14 cm^{-1} for both absorption and fluorescence transitions) to reveal features from individual (absorption, fluorescence) transition pairs. The region shown is that denoted by rectangle 3 in Fig. 3 and shows features belonging to the (^{rr}R, ^{pr}P)|(^{rp}R, ^{pp}P) and (^{rr}R, ^{rp}P)|(^{pr}R, ^{pp}P) series. K_a bandheads of the (^{rr}R, ^{pr}P)|(^{rp}R, ^{pp}P) series are seen for $K_a = 39$ to 43 and are labeled with their initial K_a value. J bandheads of the (^{rr}R, ^{rp}P)|(^{pr}R, ^{pp}P) series are seen for $J = 109$ to 120 and are labeled with their initial J value. See text for a more detailed description of these series.

To determine the value of ΔA, the bandhead positions of the (^{rr}R, ^{pr}P)|(^{rp}R, ^{pp}P) series in the experimental and calculated images were compared. Rectangle 3 in Fig. 3 encompasses a portion of this series, and this region is shown as a high resolution simulation in Fig. 9. The series head for this series of transitions is given by (^{rr}R($\kappa_{\kappa,0}$), ^{pr}P) | (^{rp}R($\kappa_{\kappa,1}$), ^{pp}P) where κ represents the K_a value of the initial rotational state prior to absorption. The next member in the series has an unchanged K_a value, but both J and K_c increase by one. The high resolution image of Fig. 9 is labeled with the K_a values located above the head of each series. In our experimental images, series with differing K_a values are fully resolved from each other as shown in Fig. 1. The useful feature of these series is that the position (absorption and fluorescence energy) of the series head is almost solely dependent on the value of ΔA. Higher members within each series are affected by ΔB and ΔC, resulting in different curvatures of these series in the 2D-LIF images; however, the series head remains fixed.

ΔB was determined by analyzing the shape of three different subseries; the (^{pp}P, ^{rp}Q) series, the (^{pr}Q, ^{rp}Q) series and the (^{pt}R,^{pr}P)|(^{pr}R,^{pp}P) series. One component of the last mentioned series results from a $\Delta K_c = 3$ transition that we label, in terms of K_c, as a T transition following conventional labeling customs. All these series show K_a fine structure whose position in the 2D-LIF images varies significantly with ΔB, and to some extent, the other rotational constants also. Thus, fitted values for ΔA (from above) and ΔC (see below) are required prior to fitting for ΔB. Rectangle 1 in Fig. 3 highlights a section of the (^{pp}P, ^{rp}Q) and (^{pr}Q, ^{rp}Q) series. Details of the transitions in this series are shown in Fig. 10. Features pertaining to these series occur in a region where there are many underlying transitions, so Fig. 10 only shows the transitions belonging to the series of interest. On this plot, the area of each marker is proportional to the intensity of the transition and the lines link different members of the series having the same K_a value. The (^{pp}P, ^{rp}Q) subseries starts off degenerate

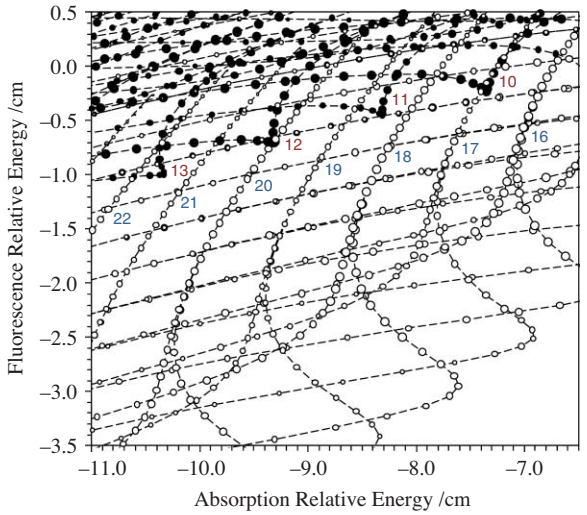

FIG. 10. Representation of a 2D-LIF image in the region denoted by rectangle 3 in Fig. 3. For clarity, only transitions of the (^{pp}P, ^{rp}Q) series (filled circles) and (^{pr}Q, ^{rp}Q) series (open circles) are shown. The area of each marker represents the intensity of the (absorption, fluorescence) transition. Turning points for the (^{pp}P, ^{rp}Q) series are observed for K_a values 10 to 13 and are labeled. K_a values ranging between 16 and 22 are shown for the (^{pr}Q, ^{rp}Q) series. Dashed lines join series members having the same K_a value. See text for a more detailed description of these series.

with the (^{pr}P, ^{rp}Q) series, where the series head (not seen in Fig. 10) is given as (^{pr}P($\kappa_{\kappa,0}$), ^{rp}Q) | (^{pp}P($\kappa_{\kappa,1}$), ^{rp}Q). Here, again, κ represents the initial K_a value for the series and increasing J and K_c by one gives the next member in the series. The two subseries continue to higher J's until they split due to asymmetry. After splitting, the difference between the absorption energies of sequential series members of the odd subseries, that is the (^{pp}P, ^{rp}Q), starts to reduce and approaches zero. Concurrent with this, the change in fluorescence transition energies as a function of J reverses from initially decreasing to increasing with J. These two behaviors of the subseries result in a build up of transitions at a particular (absorption, fluorescence) position in the 2D-LIF image, thus producing the fine structure observed in the experimental image. In Fig. 10, this effect is clearly seen for the (^{pp}P, ^{rp}Q) subseries with K_a values between 10 and 13. The "cusp" in this subseries occurs at $J = 30$ for the $K_a = 10$ series and $J = 41$ for the $K_a = 13$ series.

The second series used to determine ΔB is the (^{pr}Q, ^{rp}Q) series. Both the even and odd subseries are members of (^{pr}Q, ^{rp}Q). The series head is given by (^{pr}Q($\kappa_{\kappa,0}$), ^{rp}Q) | (^{pr}Q($\kappa_{\kappa,1}$), ^{rp}Q), with the next member in the series increasing J and K_c by one. These series are also shown in Fig. 10 where the series are labeled with their K_a value. The two subseries continue as a degenerate pair until they start to split. In the region of this splitting, the absorption energies of sequential series members for the even subseries reverses. This, coupled with favorable absorption intensity in this region, results in the fine structure observed in the image.

The remaining series used to determine ΔB is the (^{pt}R, ^{pr}P)|(^{pr}R, ^{pp}P) series, a section of which is shown in rectangular region 2 in Fig. 3. Although occurring in a region of the image that is dense with rotational transitions, this series produces well defined K_a structure whose positions are sensitive to ΔB. The bandhead of this series is given by (^{pt}R($\kappa_{\kappa,0}$), ^{pr}P)|(^{pr}R($\kappa_{\kappa,1}$), ^{pp}P) and each subsequent member increases J and K_c by one. These bandheads carry very little intensity due to low Hönl London factors, and it is the intermediate values of J (that is, before splitting occurs) that give rise to the observed structure.

ΔC was determined by the shape of the (^{rr}R, ^{rp}P)|(^{pr}R, ^{pp}P) series. This series is also influenced by ΔA, which must be determined first. The high resolution calculated image of Fig. 9 shows this series. Unlike all the series described thus far, this one is not a K_a series, but instead is a series in J. For a given J, each subseries has the first member as (^{rr}R($J_{0,J}$), ^{rp}P) | (^{pr}R($J_{1,J}$), ^{pp}P). Although the subseries can be described by sequential members having the same J value but increasing K_a values, analysis of the simulated high resolution 2D-LIF image shows this is not the most visually apparent pattern formed. The most obvious pattern is the series whose members are closest together (i.e., separated by the least energy). Therefore, we describe the subseries as transitions where subsequent members are found by decreasing J by one, increasing K_a by one and decreasing K_c by two. Using this description of the series of transitions, the initial J values are shown on Fig. 9.

[1] See special issue of Acc. Chem. Res. "Coherent multidimensional optical spectroscopy," **42**(9) (2009).
[2] M. Cho, Chem. Rev. **108**, 1331 (2008).
[3] P. C. Chen, J. Phys. Chem. A **114**, 11365 (2010).
[4] A. Schmaunz, U. Kensy, A. Slenczka, and B. Dick, Phys. Chem. Chem. Phys. **11**, 7115 (2009).
[5] N. J. Reilly, T. W. Schmidt, and S. H. Kable, J. Phys. Chem. A **110**, 12355 (2006).
[6] K. Rademann, B. Brutschy, and H. Baumgärtel, Chem. Phys. **80**, 129 (1983).
[7] G. Lembach and B. Brutschy, J. Chem. Phys. **107**, 6156 (1997).
[8] H. Shinohara, S. Sato, and K. Kimura, J. Phys. Chem. A **101**, 6736 (1997).
[9] E. D. Lipp and C. J. Seliskar, J. Mol. Spectrosc. **87**, 242 (1981).
[10] E. D. Lipp and C. J. Seliskar, J. Mol. Spectrosc. **87**, 255 (1981).
[11] N. Gonohe, H. Abe, N. Mikami, and M. Ito, J. Phys. Chem. **87**, 4406 (1983).
[12] P. Butler, D. B. Moss, H. Yin, T. W. Schmidt, and S. H. Kable, J. Chem. Phys. **127**, 094303 (2007).
[13] I. Pugliesi, N. M. Tonge, and M. C. R. Cockett, J. Chem. Phys. **129**, 104303 (2008).
[14] Z. Kisiel, E. Bialkowska-Jaworska, and L. Pszczolkowski, J. Mol. Spectrosc. **232**, 47 (2005).
[15] G. H. Kirby, Mol. Phys. **19**, 289 (1970).
[16] M. Auzinsh and R. Ferber, *Optical Polarization of Molecules* (Cambridge University Press, Cambridge, 1995).
[17] C. M. Western, PGOPHER, a Program for Simulating Rotational Structure, University of Bristol, http://pgopher.chm.bris.ac.uk.
[18] See supplementary material at http://dx.doi.org/10.1063/1.3578174 for an animated GIF file comparing experimental and computed images.
[19] Z. Kisiel, PMIFST, a Program to Calculate Principal Moments of Inertia from Molecular Structure, Institute of Physics Polish Academy of Sciences, http://info.ifpan.edu.pl/~kisiel/prospe.htm.
[20] C. Hättig and F. Weigend, J. Chem. Phys. **113**, 5154 (2000).
[21] E. D. Lipp and C. J. Seliskar, J. Mol. Spectrosc. **73**, 290 (1978).
[22] R. Vasudev and J. C. D. Brand, J. Mol. Spectrosc. **75**, 288 (1979).
[23] J. R. De Laeter, J. K. Bohlke, P. De Bievre, H. Hidaka, H. S. Peiser, K. J. R. Rosman, and P. D. P. Taylor, Pure Appl. Chem. **75**, 683 (2003).
[24] O. Dimopoulou-Rademann, K. Rademann, B. Brutschy, and H. Baumgärtel, Chem. Phys. Lett. **101**, 485 (1983).
[25] G. H. Kirby, Mol. Phys. **18**, 371 (1970).